JOURNAL OF GUIDANCE, CONTROL, AND DYNAMICS
Vol. 32, No. 5, September–October 2009

Multimodal Pilot Control Behavior in Combined Target-Following Disturbance-Rejection Tasks

P. M. T. Zaal,* D. M. Pool,† M. Mulder,‡ and M. M. van Paassen§
Delft University of Technology, 2600 GB Delft, The Netherlands

DOI: 10.2514/1.44648

Investigating how humans use their perceptual modalities while controlling a vehicle is important for the design of new control systems and the optimization of simulator motion cueing. For the identification of separate pilot response functions to the different perceived cues, multiple forcing functions need to be inserted into the manual control loop. An example of a task with multiple forcing functions is a combined target-following disturbance-rejection task, where a target and disturbance signal are used to separate the human visual and vestibular motion responses. The use of multiple forcing functions, however, also affects the nature of the control task and how the motion cues are used by the pilot to form a proper control action. This paper presents the results of an experiment where possible effects of using multiple forcing functions on pilot control behavior in an aircraft pitch control task are investigated. The results indicate that pilot performance and control activity are significantly lower when the relative power of the target forcing function is increased. This is caused by a significant change in multimodal pilot control behavior. With an increase in relative target power, the visual-perception gain is reduced and the visual time delay becomes higher. The motion-perception gain reduces if both forcing functions have significant power. It is also found that multimodal pilot control behavior in a pure target or disturbance task can be analyzed by adding a small additional disturbance or target signal, respectively. In this case, the effects on control behavior are found to be minimal, while still being able to accurately estimate the parameters of the multichannel pilot model.

Nomenclature

A	=	sinusoid amplitude, deg
e	=	tracking error signal, deg
f	=	forcing function signal, deg
f_d	=	disturbance forcing function, deg
f_t	=	target forcing function, deg
$H(j\omega)$	=	frequency response function, -
$H(s)$	=	transfer function, -
J	=	criterion function, rad^2
K_m	=	motion-perception gain, -
K_n	=	remnant intensity, -
K_v	=	visual-perception gain, -
N	=	number of points, -
n	=	pilot remnant signal, deg
n_d	=	disturbance forcing function frequency integer factor, -
n_t	=	target forcing function frequency integer factor, -
p	=	relative forcing function power, -
Q	=	optimal control performance weighting factor, -
R	=	optimal control effort weighting factor, -
s	=	Laplace variable, -
T_{A1}, T_{A2}	=	forcing function filter time constants, s
T_{lag}	=	visual lag time constant, s
T_{lead}	=	visual lead time constant, s
T_{sc1}, T_{sc2}, T_{sc3}	=	semicircular-canal time constants, s
T_m	=	measurement time, s
t	=	time, s
u	=	pilot control signal, deg
δ_e	=	elevator deflection, deg
ζ_n	=	remnant filter damping, -
ζ_{nm}	=	neuromuscular damping, -
θ	=	pitch angle, deg
σ	=	standard deviation
τ_m	=	motion-perception time delay, s
τ_v	=	visual-perception time delay, s
φ_m	=	phase margin, deg
ϕ	=	sinusoid phase shift, rad
ω	=	frequency, rad s^{-1}
ω_c	=	crossover frequency, rad s^{-1}
ω_n	=	remnant filter break frequency, rad s^{-1}
ω_{nm}	=	neuromuscular frequency, rad s^{-1}

Subscripts

d	=	disturbance
t	=	target

Presented as Paper 6027 at the AIAA Modeling and Simulation Technologies Conference, Chicago, IL, 10–13 August 2009; received 31 March 2009; revision received 15 May 2009; accepted for publication 18 May 2009.

*Ph.D. Candidate, Control and Simulation Division, Faculty of Aerospace Engineering, Post Office Box 5058; p.m.t.zaal@tudelft.nl. Student Member AIAA.

†Ph.D. Candidate, Control and Simulation Division, Faculty of Aerospace Engineering, Post Office Box 5058; d.m.pool@tudelft.nl. Student Member AIAA.

‡Professor, Control and Simulation Division, Faculty of Aerospace Engineering, Post Office Box 5058; m.mulder@tudelft.nl. Member AIAA.

§Associate Professor, Control and Simulation Division, Faculty of Aerospace Engineering, Post Office Box 5058; m.m.vanpaassen@tudelft.nl. Member AIAA.

I. Introduction

IN MOST vehicular control tasks, human operators use multiple cues to achieve a proper control action. For example, in an aircraft pitch control task, pilots visually perceive the pitch angle from their primary flight display and, due to the physical aircraft pitch rotation, also sense changes in aircraft pitch with their vestibular system [1]. In a skill-based continuous control task, these cues are processed by the central nervous system, where appropriate weight is put on visual and vestibular responses. Modeling this process can give insight into the relative importance of the different motion cues and is important in, for example, flight simulator fidelity research. As the simulation

of motion cues is constrained by the limitations of the simulator, such knowledge can be used to optimize simulator motion cueing [2].

When modeling the perceptual modalities of the pilot, a multichannel model is often used that takes the perceived cues as inputs. The output of this quasi-linear model is the summation of pilots' linear responses to each perceived cue, supplemented with a remnant signal that accounts for the nonlinear behavior [3,4]. The linear response functions consist of sensor dynamics, gains, time constants, time delays, and neuromuscular dynamics. For accurate estimation of these parameters, current identification techniques require the different inputs of the model to be uncorrelated and sufficiently exciting. To achieve this, an independent forcing function signal is inserted into the closed-loop system for every pilot-model input [4–7]. The location where the forcing functions are inserted into the closed-loop system, and the intensity of the individual forcing functions, can affect the task of the pilot and how the different motion cues are used in the control task.

Two classical types of manual control tasks that are frequently studied in literature are disturbance-rejection and target-following tasks. Motion cues have been shown to have different functions in these two types of tasks. In a disturbance-rejection task, the visual and vestibular inputs to the pilot are driven by the same system output, yielding a task in which the visual and vestibular modalities work in parallel. In a target-following task, the physical motion cues are directly related to the control action of the pilot, as this action is the only input to the controlled dynamics. Different effects of motion cues on pilot control behavior in disturbance-rejection and target-following tasks have indeed been observed in several experimental studies [8–11].

In these classical single forcing function tasks [3,9–14], the relation between the visual and vestibular cues and the pilot control action is evident. Reliable identification of pilots' visual and vestibular responses is, however, not possible for such tasks due to the use of only one forcing function signal. A strategy that has been used in many experiments [1,4,12,15,16] solely to facilitate multichannel pilot-model identification is to use both target and disturbance forcing functions in a combined target-following and disturbance-rejection task. In such a combined control task, the insertion of two forcing functions decreases the coherence between both cues and may introduce a cue conflict. By limiting the magnitude of the additional forcing function signal, the preferred target-following or disturbance-rejection portion of the task can be made dominant, minimizing possible cue conflicts [1,4]. However, a tradeoff has to be made, as reducing the additional signal's power below a certain level will again result in unreliable identification results.

Although the concept of using an additional forcing function with relatively low power for the modeling of multiple modalities has been used in many experiments, the minimum power of this additional signal, required for accurate estimation results, has never been determined. Additionally, it is crucial to know if adding an extra signal, even with low power, significantly changes control behavior compared to the single forcing function tasks. These topics are studied in this paper.

An experiment was performed in the SIMONA Research Simulator (SRS) of the Delft University of Technology in which the influence of multiple forcing functions on pilot performance and control behavior is investigated for an aircraft pitch control task. For this purpose, the relative power of the target and disturbance forcing functions was systematically varied over the different experimental conditions. In a similar experiment studying the same topics for a double-integrator roll control task, no significant effect on multimodal pilot control behavior was found. Tracking performance and control activity, however, were found to be significantly affected [17]. The use of more accurate identification techniques for the estimation of the pilot-model parameters [7] for the experiment discussed in the current paper may yield new insights into how pilot control behavior is affected.

The paper is structured as follows. First, the multimodal pilot modeling procedure used in this research will be discussed. Next, an optimal control analysis is presented, which was performed to gain some insight into the theoretically optimal use of motion cues for a systematic change in relative power of target and disturbance forcing functions. After this, the experiment setup and results will be discussed. The paper ends with a discussion and conclusions.

II. Multimodal Pilot Modeling

Pilot manual control behavior in skill-based continuous control tasks can be described by relatively simple control-theoretic pilot models [3]. For vehicle control tasks in which pilots use multiple perceptual modalities (for instance, visual and vestibular), modeling of control behavior is, however, not straightforward and poses requirements on the forcing functions that are used to induce control actions [4–7]. This section describes the control task, multichannel pilot model and forcing functions used in this paper for investigating how changes in relative target and disturbance signal power affect multimodal pilot control behavior and its identification from measurement data.

A. Control Task

The closed-loop compensatory aircraft pitch attitude control task studied in the experiment described in this paper is depicted in Fig. 1. This control task is similar to the task used in a previous experiment, in which the influence of pitch and heave motion cues on multimodal pilot control behavior was investigated [1].

For the controlled aircraft pitch dynamics, indicated with H_{θ,δ_e} in Fig. 1, a linearized model of the Cessna Citation I Ce500, trimmed at an altitude of 10,000 ft and a true airspeed of 160 kt, is used. The transfer function for these dynamics is given by

$$H_{\theta,\delta_e}(s) = -10.6189\frac{s + 0.9906}{s(s^2 + 2.756s + 7.612)} \tag{1}$$

A Bode plot of the controlled dynamics is given in Fig. 2. As indicated in the figure by the gray lines, the controlled aircraft dynamics resemble those of a single integrator for frequencies below 1 rad/s and a double integrator for frequencies above 3 rad/s. Between 1 rad/s and the short period peak at $\omega_{sp} = 2.76$ rad/s the dynamics approximate a gain.

For identification of both pilot visual and vestibular responses (H_{pe} and $H_{p\theta}$ in Fig. 1), two forcing functions need to be inserted into the closed-loop control task. A target forcing function f_t is inserted by displaying the error e between the target and the actual pitch angle θ on a visual compensatory display. A disturbance forcing function f_d is used as a physical disturbance on the aircraft dynamics. Pitch rotational motion is generated by the simulator motion base and may be perceived by the pilot through his vestibular system. The heave motion cues associated with a change in aircraft pitch attitude [1] were not provided by the simulator.

If the power of the target is zero, the task is a pure disturbance task and the visual and physical motion cues, that is, the two inputs of the pilot in Fig. 1, are similar. If the power of the disturbance is zero, the task is a pure target task. In this case, the pilot control signal is the only input to the controlled dynamics and the target signal induces a difference between the information that is present in the visual and physical motion cues.

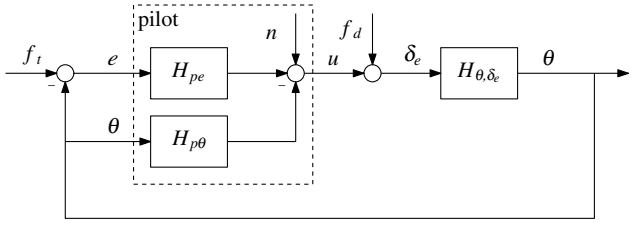

Fig. 1 Schematic representation of a closed-loop compensatory aircraft pitch control task.

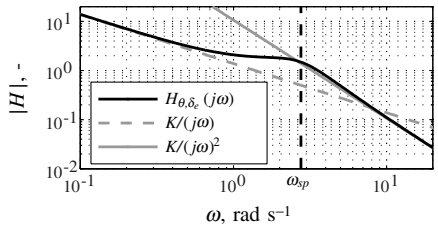

a) Magnitude

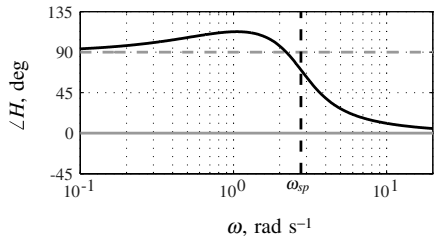

b) Phase

Fig. 2 Bode plots of controlled aircraft dynamics.

B. Multimodal Pilot Model

The structure of an appropriate multimodal pilot model for the control task given in Fig. 1 is given in Fig. 3. The model contains a visual and a vestibular input (e and θ) and two parallel channels (H_{pe} and $H_{p\theta}$) to model the visual and vestibular modalities separately [9]. A remnant signal n is added to the output of the linear channels to account for the nonlinear behavior of the pilot.

Human operators adapt their control behavior to the controlled dynamics H_{θ,δ_e} in such a way that the open-loop dynamics in the crossover region can be described by a single integrator and a time delay [3]. With the aircraft pitch dynamics as depicted in Fig. 2 and typical crossover frequencies between 2 and 4 rad/s for this type of control task, the pilot needs to generate lag to compensate for the gain dynamics around the short period frequency. Subsequently, a quadratic lead term is needed to compensate the lag and to achieve the required lead compensation for the double-integrator dynamics at higher frequencies [1]. This results in the pilot equalization given in Fig. 3.

The visual-perception channel H_{pe} contains the visual-perception gain K_v, a visual lead time constant T_{lead}, a visual lag time constant T_{lag}, and a visual-perception time delay τ_v. The pitch motion-perception channel $H_{p\theta}$ includes the dynamics of the semicircular canals H_{sc}, the motion-perception gain K_m, and a motion-perception time delay τ_m. In both channels, the control action of the pilot is affected by the neuromuscular dynamics H_{nm}, given by

$$H_{nm}(j\omega) = \frac{\omega_{nm}^2}{\omega_{nm}^2 + 2\zeta_{nm}\omega_{nm}j\omega + (j\omega)^2} \tag{2}$$

with ζ_{nm} the neuromuscular damping and ω_{nm} the neuromuscular frequency. The semicircular-canal dynamics in the pitch motion-perception channel are given by

$$H_{\text{sc}}(j\omega) = \frac{1 + j\omega T_{\text{sc1}}}{(1 + j\omega T_{\text{sc2}})(1 + j\omega T_{\text{sc3}})} \tag{3}$$

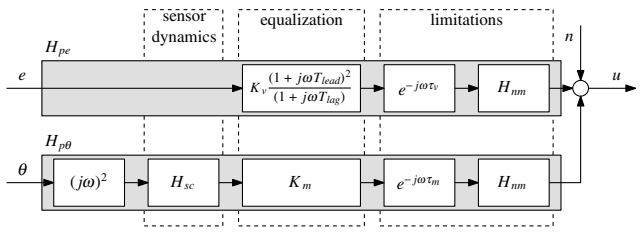

Fig. 3 Multichannel pilot-model structure.

with $T_{\text{sc1}} = 0.11$ s, $T_{\text{sc2}} = 5.9$ s, and $T_{\text{sc3}} = 0.005$ s the time constants of the semicircular-canal model. These values are taken from previous research [10] and are fixed in the parameter estimation procedure. Note that due to the integrating action of the semicircular-canal dynamics as defined by Eq. (3), the vestibular channel effectively provides a second source of lead information in addition to the contribution of the visual lead constant, T_{lead}. A portion of the required lead generation may thus be taken over by a pilot's vestibular system if motion cues are available. A significant reduction in visual lead time constant when physical motion cues were made available has been observed in previous experiments where similar control tasks were considered [1].

With the time constants of the semicircular-canal model kept constant, a total of eight pilot-model parameters are left to be estimated (K_v, T_{lead}, T_{lag}, τ_v, K_m, τ_m, ζ_{nm}, and ω_{nm}).

C. Forcing Functions

For the closed-loop pitch attitude control task as defined in Fig. 1, the target and disturbance signals are designed as quasi-random sum-of-sine signals with sines at multiple frequencies. The random appearance of such multisine signals induces skill-based feedback control behavior, while allowing the experiment designer to accurately define the forcing function properties in the frequency domain. The forcing functions were generated according to

$$f_{d,t}(t) = \sqrt{p_{d,t}} \sum_{k=1}^{N_{d,t}} A_{d,t}(k) \sin[\omega_{d,t}(k)t + \phi_{d,t}(k)] \tag{4}$$

where the subscripts d and t indicate the disturbance or target forcing function, respectively. In Eq. (4), $A(k)$, $\omega(k)$, and $\phi(k)$ indicate the amplitude, frequency, and phase of the kth sine in f_d or f_t. N indicates the number of sines in the signals and p is the relative power fraction, which is between 0 and 1. Both f_d and f_t consisted of 10 individual sinusoids, but each had a different amplitude, frequency, and phase distribution.

The measurement time of an individual experimental measurement run is $T_m = 81.92$ s. The sinusoid frequencies $\omega_d(k)$ and $\omega_t(k)$ were all integer multiples of the measurement time base frequency, $\omega_m = 2\pi/T_m = 0.0767$ rad/s. The selected sinusoid frequencies and the corresponding integer factors of ω_m, n_d and n_t, can be found in Table 1.

To determine the amplitudes of the individual sines for both the target and the disturbance forcing function, a second-order low-pass filter was used:

$$H_A(j\omega) = \left(\frac{1 + T_{A1}j\omega}{1 + T_{A2}j\omega}\right)^2 \tag{5}$$

with $T_{A1} = 0.1$ s and $T_{A2} = 0.8$ s. The absolute value of the filter at a sinusoid frequency gives the corresponding sinusoid amplitude. The reduced magnitude of the amplitudes at the higher frequencies yields a tracking task that is not overly difficult. The amplitude distributions $A_d(k)$ and $A_t(k)$ were scaled to attain equal variances for f_d and f_t of 2.0 deg^2.

To determine the forcing function phase distributions, a large number of random sets of phases were generated. The two sets of phases that yielded signals with a probability distribution closest to a Gaussian distribution, without leading to excessive peaks, were selected for f_d and f_t [18].

The disturbance signal was inserted into the closed-loop control task *before* the controlled aircraft dynamics by adding it to the pilot's control signal u, as can be verified from Fig. 1. Therefore, the disturbance signal amplitudes and phases need to be prefiltered with the inverse of the aircraft model pitch response $H_{\theta,\delta_e}(j\omega)$. This ensured that f_d had similar properties as f_t after passing the controlled dynamics.

In this research, the relative power of both forcing functions is varied between different experimental conditions. The total power inserted by the forcing functions is always equal to 2.0 deg^2. This implies that the following relation for the relative power of the

Table 1 Experiment forcing function properties

Disturbance, f_d				Target, f_t			
n_d, –	ω_d, rad s^{-1}	A_d, deg	ϕ_d, rad	n_t, –	ω_t, rad s^{-1}	A_t, deg	ϕ_t, rad
5	0.383	0.385	−0.269	6	0.460	1.562	1.288
11	0.844	0.505	4.016	13	0.997	1.092	6.089
23	1.764	0.308	−0.806	27	2.071	0.493	5.507
37	2.838	0.201	4.938	41	3.145	0.265	1.734
51	3.912	0.212	5.442	53	4.065	0.178	2.019
71	5.446	0.263	2.274	73	5.599	0.110	0.441
101	7.747	0.352	1.636	103	7.900	0.070	5.175
137	10.508	0.483	2.973	139	10.661	0.051	3.415
171	13.116	0.635	3.429	194	14.880	0.040	1.066
226	17.334	0.949	3.486	229	17.564	0.036	3.479

disturbance and target holds: $p_d = 1 - p_t$, where p_t varies between zero and one. For $p_t = 0$, the target will be zero and the control task will be a pure disturbance task. For $p_t = 1$ all forcing function power in the control loop will be provided by the target forcing function and the task will be a pure target task. Because of this relation between relative target and disturbance power, it should be noted that when an increase in target power is mentioned in the paper without any mention about the disturbance power, the disturbance power consequently decreases.

Figure 4 depicts a part of a time trace for both forcing function signals with p_d and p_t equal to 1. Note that the disturbance signal as depicted in the figure is the signal prefiltered with the inverse of the controlled dynamics. The properties of the target and disturbance signals are summarized in Table 1.

III. Optimal Control Analysis

An optimal control analysis was performed to determine the theoretically optimal pilot-model settings for a change in relative power of the forcing functions. For this analysis, the target and disturbance forcing function power is systematically varied between 0 and 100%; that is, the task is changed from a pure disturbance task to a pure target task, with combined target-following disturbance-rejection tasks in between. Because of the different role motion cues play in target following and disturbance rejection, optimal weighting of pilot visual and vestibular responses, for instance in the generation of pilot lead, may be different for both tasks. This analysis will give some insight into the optimal use of visual and physical motion cues for the different forcing function power settings.

A. Setup of the Optimal Control Analysis

In the optimal control analysis, the closed-loop control structure depicted in Fig. 1 is used. The pilot is represented by the full pilot model given in Fig. 3. The control law for this optimal control problem is given by

$$u = H_{pe}e - H_{p\theta}\theta + H_n n \tag{6}$$

with n a zero mean Gaussian white noise signal and H_n the remnant filter given by

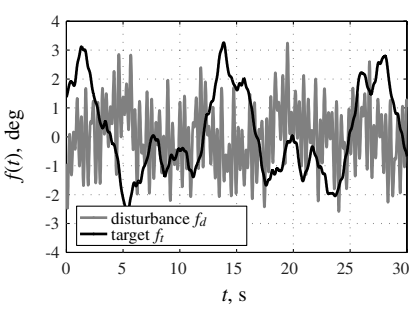

Fig. 4 Time trace of the disturbance and target forcing function signals ($p_d = p_t = 1$).

$$H_n(j\omega) = \frac{K_n\omega_n^3}{((j\omega)^2 + 2\zeta_n\omega_n j\omega + \omega_n^2)(j\omega + \omega_n)} \tag{7}$$

The parameters in the remnant filter are the remnant intensity K_n, the remnant break frequency ω_n, and a damping coefficient ζ_n. This remnant filter characteristic was found experimentally in previous research [7]. The parameters in the optimal control law are computed by minimizing the following criterion function:

$$J = \underbrace{Q\sigma^2(e)}_{\text{performance}} + \underbrace{R\sigma^2(u)}_{\text{effort}} \tag{8}$$

In the criterion function, the constant factors Q and R control the relative weighting of the minimization of the variance of the error (tracking performance) and the variance of the control signal (control effort), respectively.

As the optimization problem is highly overdetermined (the pilot model, including the remnant filter consists of 11 parameters), some parameters need to be fixed. As the change in relative forcing function power will change the relation between the different pilot-model inputs, it is expected that the equalization of the pilot model will be mostly affected. For this reason the parameters of the pilot equalization are optimized, while the rest of the parameters are fixed. The values of these fixed parameters are as follows: $\tau_v = 0.27$ s, $\tau_m = 0.18$ s, $\zeta_{nm} = 0.18$, $\omega_{nm} = 11.56$ rad s^{-1}, $K_n = 4.0$, $\zeta_n = 0.26$, and $\omega_n = 12.7$ rad s^{-1}. The parameters are taken from a previous human-in-the-loop experiment performed in the SRS, in which the same aircraft pitch control task was performed [1,7]. The forcing functions in this experiment were identical to the ones defined in Sec. II.C, with $p_t = 0.2$ and $p_d = 0.8$. The selected value for the remnant intensity K_n ensures that 10% of the variance of the control signal is caused by the remnant, as found in previous research [1].

The optimal values for the visual-perception gain K_v, the motion-perception gain K_m, and the visual lead time constant T_{lead} are determined by minimizing J as defined by Eq. (8). The lag time constant T_{lag} was set to $2.4T_{\text{lead}}$. This approximate relation was also found for the experiment mentioned previously [1] and further increases the probability of finding an optimal solution of the optimization problem. The weighting factors Q and R of the cost function were determined to provide values of K_v, T_{lead}, T_{lag}, and K_m that were very close to those found for the experiment described in [1]. The values for Q and R were set to 10 and 1, respectively.

B. Results

The results of the optimal control analysis are depicted in Figs. 5 and 6. Figure 5 gives the optimal values of K_v, T_{lead}, and K_m for a change in forcing function power given the assumed control structure. The vertical line at $p_t = 0.2$ indicates the condition of the experiment in [1], of which the data are taken for the fixed parameters. From a pure disturbance to a pure target task (p_t from 0 to 1), the visual and motion-perception gains decrease. As lead information can result from either the integrating action of the semicircular canals, the visual lead, or a combination of these, a

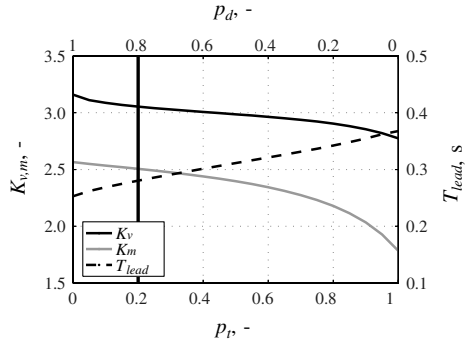

Fig. 5 Visual and motion gains, and visual lead time constant for change in relative forcing function power.

consequence of the decrease of the motion gain is an increase in the visual lead time constant, as is also observed in Fig. 5.

Figure 6 gives the variance of the error signal and the variance of the control signal, the pilot performance and control activity, respectively. It can be seen that tracking performance decreases (the variance of the error increases) and the control activity remains approximately constant, as the control task is changed from pure disturbance rejection to pure target following.

C. Discussion

For a pure disturbance task ($p_t = 0$), the visual and physical motion cues are equal. Because of this, and the fact that using motion cues is a faster and more efficient way of generating lead (due to the smaller motion-perception time delay, see Sec. III.A), it can be expected that the perception gains are relatively high and the visual lead is minimized. For a target task ($p_t = 1$), the inputs to the pilot model are not equal, that is, a cue conflict is introduced. It can be expected that this results in a decrease of the perception gains and an increase in visual lead, as lead information on the forcing function is only available visually. The results found for the optimal parameters in Fig. 5 support this.

Figure 6 indicates that the tracking performance is higher for a disturbance task than for a target task. This is a result of the increased perception gains for the disturbance task. The same result was found in previous research that investigated the effect of different motion cues on target and disturbance tasks [9]. A logical consequence of the increase in performance would be an increase in control activity. This result is, however, not found in the optimal control analysis. Rather, a minimal increase in control activity can be observed.

IV. Experiment

To verify whether the differences in theoretically optimal control behavior for target following and disturbance rejection as observed from the optimal control analysis indeed represent typical trends for human manual control behavior, a human-in-the-loop experiment was performed. This experiment was designed to reveal possible

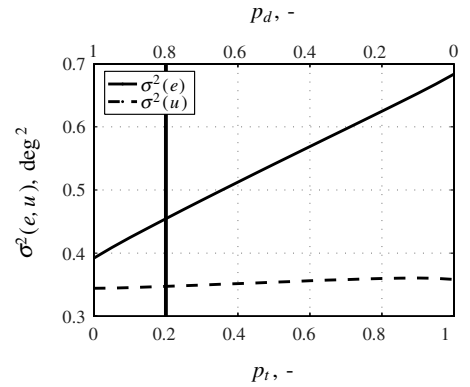

Fig. 6 Error and control signal variance for a change in relative forcing function power.

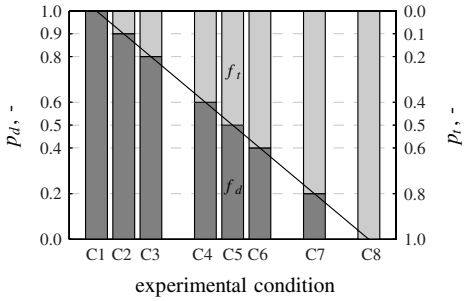

Fig. 7 Graphical representation of the eight experimental conditions.

trends in manual control behavior when varying forcing function settings from pure target to pure disturbance, and to compare control behavior for relative target and disturbance forcing function power settings as used in some previous experiments [1,2,4,6,16,19,20] to control behavior for pure target-following and disturbance-rejection tasks.

A. Method

The experiment performed for this research was highly similar to the experiment described in [1]. As stated in Sec. II, the same controlled element dynamics and quasi-random forcing function signals were used in both experiments. Further important details of the current experiment are described next.

1. *Independent Variables*

This experiment was designed to evaluate the effect of varying a single independent variable: the proportion of target and disturbance forcing function power in a compensatory control task. The eight conditions of this experiment, numbered C1 to C8, are depicted in Fig. 7. The dark gray portions of the bars in this graph indicate the percentage of disturbance forcing function power for each condition; the (upper) light gray portions indicate the percentage of power accounted for by f_t. The experimental conditions were selected to be very similar to those evaluated in an earlier experiment [17].

As physical motion cues most significantly affect pilot control behavior in a pure disturbance-rejection task, in many earlier piloted tracking experiments where different modalities were modeled separately, a disturbance-rejection task was used with an additional target signal that had 20% of the total forcing function power [1,2,4,6,16,19,20]. This relative forcing function power distribution is represented by condition C3 in Fig. 7. To investigate if further reduction of the target forcing function power would yield a task for which multimodal pilot-model identification is still possible, condition C2 was added. For a pure disturbance-rejection task the pilot-model inputs are the same, yielding a highly overdetermined identification problem. As this problem is less severe for a pure target task, where the pilot inputs are not similar, no condition was added between C7 and C8.

2. *Apparatus*

The experiment was performed in the SRS at Delft University of Technology (see Fig. 8). Rotational pitch motion cues were provided

Fig. 8 The SIMONA research simulator.

by the 6 degree-of-freedom hydraulic hexapod motion system during all experiment runs. No washout filter was used and controlled element pitch attitudes were presented 1-to-1. The center of rotation was located at the upper gimbal point (UGP) of the simulator. The UGP is located 1.2075 m below the design eye reference point, that is, 1.2075 m below the approximate location of the pilot's head. No heave motion cues were provided. The time delay associated with the response of the SRS motion system has been experimentally determined to be approximately 30 ms [21].

During the experiment, subjects were seated in the right pilot seat. They controlled the Citation pitch dynamics using an electrical side stick without breakout force and a maximum pitch deflection of 14 deg. Stick stiffness was set to 1.1 N/ deg for deflections below 9 deg; at higher stick deflections the stiffness was increased to 2.6 N/ deg. A simplified artificial horizon image (Fig. 9) was projected on the right primary flight display in the SRS cockpit to indicate the tracking error e, which subjects were to minimize during the experiment. The primary flight display had an update rate of 60 Hz and a time delay (including the projection) of no more than 25 ms.

3. *Participants and Instructions*

Seven subjects were invited to perform this experiment. All participants were male and their ages ranged from 23 to 47 years old. Four of the participants were university staff members, who all had experience as pilots of single or multi-engine aircraft. Two of them were active Citation II pilots. The remaining three participants were students at the Faculty of Aerospace Engineering. One of these students had 119 flight hours in single engine aircraft; the others had experience with manual vehicle control tasks from previous human-in-the-loop experiments.

Before the start of the experiment, the objective of the experiment was explained to the participants. They were told that they would be performing a combined target-following and disturbance-rejection task and that the relative power of the target and disturbance signals would be varied over the eight different conditions depicted in Fig. 7. The main instruction the participants received was that they should attempt to minimize the pitch tracking error, that is, the signal e presented on the visual display, within their capabilities.

4. *Experimental Procedure*

An individual experiment run was defined to last 90 s, of which the final 81.92 s were used as the measurement data. Data were logged at a frequency of 100 Hz. Data from the first 8.08 s of each run were logged, but discarded for analysis. From previous experiments [1] it was known that 8 s is more than enough time for participants to stabilize the controlled aircraft dynamics after the start of a run.

During the experiment, the participants' tracking performance, expressed in terms of the root mean square of the error signal e, was recorded for each condition by the experimenter. When a participant's level of performance had clearly stabilized and six repetitions of each condition had been collected at this stable performance level, the experiment was terminated. No fixed number of training runs was defined before the experiment. On average, 9 to 10 repetitions of each experimental condition were sufficient to gather the measurement data for each subject. Typically, each subject performed 24 runs, that is, three repetitions of all conditions, in between breaks. This allowed each subject to complete the experiment in approximately 4 h.

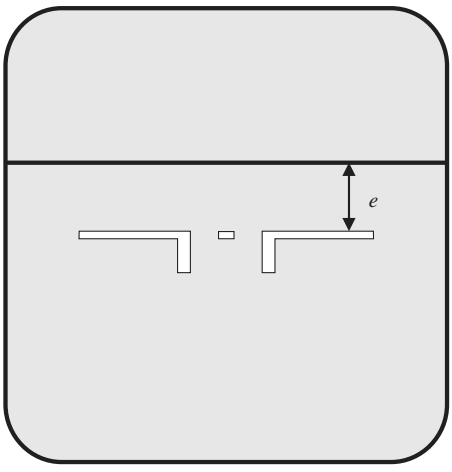

Fig. 9 Compensatory display.

The experiment had a balanced Latin square design: the eight conditions of the experiment were presented in quasi-random order. Subjects were informed of their tracking score after each run to motivate them to consistently perform the tracking task at their maximum level of performance.

5. *Dependent Measures*

To investigate the effects of a systematic variation in target and disturbance forcing function power as depicted in Fig. 7, a number of dependent measures were considered to be of interest. First of all, the variances of the recorded error signal e and control signal u were calculated as measures of tracking performance and control activity, respectively. In addition, the contributions of the target and disturbance signal power to these overall signal variances were determined using a spectral method as described in [8].

In addition to these signal properties, the multimodal pilot model given in Fig. 3 was fitted to the time-domain data using a genetic maximum likelihood (MLE) procedure [7]. The MLE method requires the inputs of the pilot model to be sufficiently exciting and informative to give accurate parameter estimates. To have sufficiently exciting model inputs depends on the control task, the controlled dynamics, and even the control strategy adopted by the subjects. This requirement was not met for the pure disturbance and target task in the current experiment, conditions C1 and C8. To accurately estimate the model parameters for these tasks, some parameters were fixed to values extrapolated from those found for neighboring conditions with two forcing functions, for which accurate estimates could be achieved, C2 and C3, and C6 and C7. Using this strategy, reliable estimation of the remaining parameters was guaranteed.

To evaluate the accuracy of the pilot model in the time domain, the variance accounted for (VAF) was calculated using the measured pilot control signal and the output of the linear pilot model [6]. The VAF gives the percentage of the measured pilot control signal variance that can be explained by the linear response functions. The remaining portion of the variance can be attributed to the pilot remnant.

Changes in pilot-model parameters were used to quantify changes in pilot control strategy. In addition, the effect of these changes in control behavior on the attenuation of the target and disturbance signals was evaluated from the target and disturbance open-loop responses, respectively [8]. In the frequency domain, pilot performance is determined by the crossover frequencies and phase margins of the different open-loop responses. Using the pilot response functions given in Figs. 1 and 3, the disturbance open-loop response is determined by

$$H_{\mathrm{ol},d}(j\omega) = \frac{U(j\omega)}{\delta_e(j\omega)} = [H_{pe}(j\omega) + H_{p\theta}(j\omega)]H_{\theta,\delta_e}(j\omega) \qquad (9)$$

and the target open-loop response function is given by

$$H_{\mathrm{ol},t}(j\omega) = \frac{\theta(j\omega)}{E(j\omega)} = \frac{H_{pe}(j\omega)H_{\theta,\delta_e}(j\omega)}{1 + H_{p\theta}(j\omega)H_{\theta,\delta_e}(j\omega)} \qquad (10)$$

For a pure target and disturbance task, only one of the open-loop frequency response functions is defined, as there is only one forcing function present. The disturbance and target crossover frequencies, $\omega_{c,d}$ and $\omega_{c,t}$, are the frequencies where the magnitude of the disturbance and target open-loop responses cross the line with a

magnitude of 1. The corresponding phase margins, $\varphi_{m,d}$ and $\varphi_{m,t}$, are the phase differences with -180 deg at the crossover frequencies.

B. Hypotheses

Previous experiments have shown that when physical motion cues are available, significantly better tracking performance and higher control activity are observed for a disturbance-rejection task compared to the target-following task [11,17]. The results of the optimal control analysis of Sec. III also show the performance increase, but indicate slightly decreased control activity for higher disturbance forcing function power levels. This disagreement between experimental and theoretical results is thought to be at least partly due to the assumptions made in the optimal control analysis. Therefore, as found in the previous experiments, tracking performance and control activity are expected to increase in the current experiment with increasing disturbance forcing function power.

For changes in manual control behavior, the optimal control analysis suggests that for increasing levels of target forcing function power, more pilot lead will be generated from visual cues. For disturbance rejection, it is better to acquire the required lead from physical motion cues instead. Therefore, an increase in the value of the visual lead constant T_{lead} and a decrease in the value of the motion gain K_m (see Sec. II.B) is expected to be found from pilot-model identification results with increasing target forcing function power. Based on the findings from the experiment described in [17], however, it is expected that the changes in control behavior over the different conditions will be relatively small in magnitude.

V. Results

This section presents the combined results of all seven subjects who participated in the experiment. A repeated-measures analysis of variance (ANOVA) was performed to identify significant trends in the data. Significant linear or quadratic trends, if present in the presented data, are indicated with gray lines in all graphs shown in this section.

A. Tracking Performance and Control Activity

The variances of the error and control signals are given in Fig. 10. For every condition the mean data over all runs of all subjects are shown. The variance is decomposed into the variance components due to the input signals of the control loop [8]. The variance components due to the target and disturbance signals can be calculated using the power spectral density functions of the error and control signals at the input frequencies of the target and disturbance forcing functions, respectively. The remnant component is the difference between the total variance in the signal and the sum of the target and disturbance components.

In Fig. 10a it can be seen that the variance of the error increases, that is, performance degrades, when the variance of the target signal is increased. The ANOVA indicates that this effect is highly significant [$F(7, 42) = 83.401$, $p < 0.05$]. The figure indicates an almost perfect linear trend across the conditions, which is confirmed by polynomial contrasts [$F(1, 6) = 131.772$, $p < 0.05$]. When inspecting the variance components, it can be seen that the variance due to the target signal increases much faster than the variance due to the disturbance decreases, causing the increase in the total variance of the error signal. The remnant variance in the error signal remains approximately constant.

To further investigate these trends in the variance of the error signal, the percentage of the variances induced by the target and disturbance signals that are compensated for by the subjects have been calculated and are given in Fig. 11. The error bar plot gives the means and 95% confidence intervals for all subjects. The data are adjusted using the subject means to compensate for the between-subject variability. Note that, as explained in Sec. II.C, the total variance inserted by the target and disturbance forcing function is 2.0 deg^2 for all conditions.

Figure 11 shows that the percentage of the variance compensated for remains constant for all conditions for both the disturbance and the target components. This result is supported by the ANOVA [$F(6, 36) = 1.390$, $p > 0.05$ and $F(6, 36) = 1.271$, $p > 0.05$]. Furthermore, it can be seen that disturbance errors are attenuated much more effectively (87%) than errors introduced by the target signal (72%), a significant effect [$F(1, 6) = 122.915$, $p < 0.05$].

In Fig. 10b the variance of the control signal shows a significant decrease if the power of the target signal is increased [$F(7, 42) = 6.131$, $p < 0.05$]. The control signal variance changes quadratically over the conditions [$F(1, 6) = 13.337$, $p < 0.05$]. The decrease in control activity results in a decrease in tracking performance as seen in Fig. 10a. This result was also found in a similar experiment [17]. It can be seen that the disturbance component in the control signal decreases much faster than the target component increases. The remnant component in the control signal remains more or less constant and contributes 40–45% of the total variance in the control signal, as also observed in previous experiments [1,6].

B. Pilot Control Behavior

For every subject and every condition, the pilot model of Fig. 3 was fit to the time-domain data using MLE. MLE requires the pilot model to be converted to a state-space representation. For this conversion the controller canonical form was used. The time delays of the model were included using fifth order Padé approximations. To reduce the influence of the remnant on the parameter estimates,

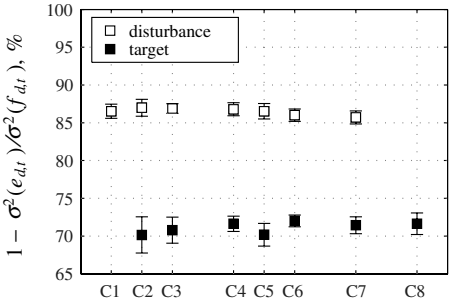

Fig. 11 Percentage of the disturbance and target variance in the error signal compensated for by the control action of the subjects.

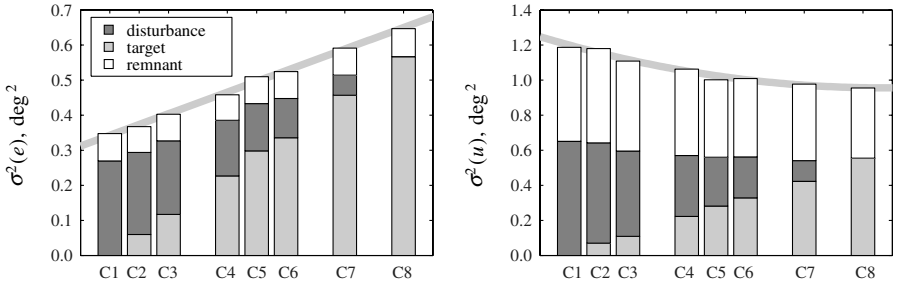

Fig. 10 Variance decomposition of the error and control signals for every condition averaged over seven subjects. The gray lines indicate significant trends.

the averaged time-domain data of five measurement runs were used as input to the MLE method.

As explained in Sec. IV.A.5, accurate parameter estimates could only be achieved for the conditions with both forcing functions having power (C2–C7). For condition C1, the visual and physical motion-perception delays were fixed. For the pure target-following task (C8), the delays and the neuromuscular frequency were fixed. The fixed parameters for the pure disturbance and target task were extrapolated from the neighboring conditions C2 and C3, and C6 and C7, respectively.

1. *Pilot-Model Parameters*

The identified pilot frequency response functions, H_{pe} and $H_{p\theta}$, for all conditions averaged over all subjects are given in Fig. 12. The observed changes in control behavior over the experimental conditions were highly similar for all subjects. As indicated by the arrow in Fig. 12a, only a clear trend in the magnitude of the pilot visual response can be observed.

The means and 95% confidence intervals of the multimodal pilot-model parameters estimated with the MLE method are given in Fig. 13. The data are adjusted for between-subject variability. Significant trends are indicated by the gray lines.

Figure 13a shows a clear decrease in visual gain as the power of the target forcing function is increased. The ANOVA shows that the effect is significant [$F(7, 42) = 8.592,\ p < 0.05$] and polynomial contrasts indicate the trend is linear [$F(1, 6) = 15.134,\ p < 0.05$]. This decreasing trend in the visual gain, which is also apparent from Fig. 12a, can be explained by the increasing cue conflict with the physical motion cues as the target power increases.

The pitch motion-perception gain first decreases as more target power is inserted into the control loop, but then increases again when the target becomes dominant, as can be seen in Fig. 13b. This effect is significant [$F(7, 42) = 3.114,\ p < 0.05$] and the trend is indeed quadratic [$F(1, 6) = 34.987,\ p < 0.05$]. The higher gain for the pure disturbance task (C1) is caused by the fact that the visual and physical motion cues are identical. Next, as the cue conflict increases due to the increasing target power (C2–C5), the relation between the two cues becomes less clear and the physical motion gain decreases. If the target power becomes dominant (C6–C7), the relation of the physical motion cues with the pilot control input becomes stronger, resulting in an increasing motion-perception gain. Finally, for the pure target-following task (C8), the motion cues are completely related to the pilot control signal and the magnitude of the motion-perception gain is almost equal to the magnitude for the pure disturbance task. This experimental result was not anticipated for by the results of the optimal control analysis.

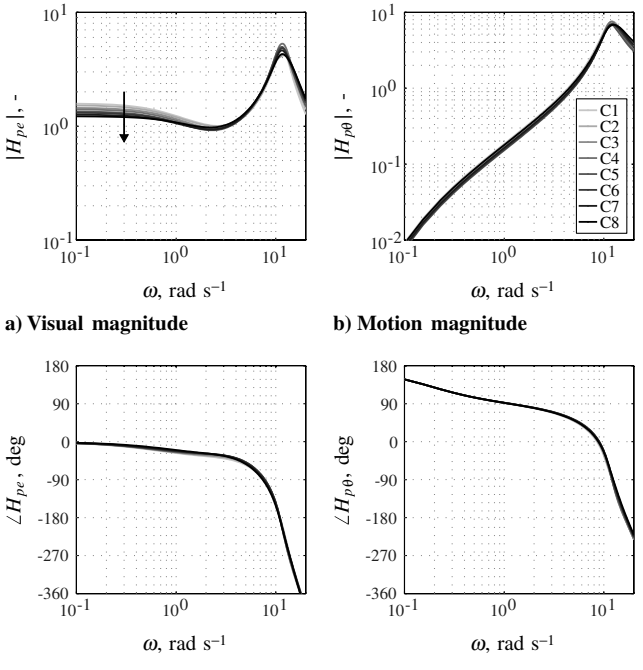

a) Visual magnitude **b) Motion magnitude**

c) Visual phase **d) Motion phase**

Fig. 12 Mean pilot visual and pitch motion frequency response functions.

Figure 13c reveals an opposite trend to the motion-perception gain for the visual lead time constant. However, this trend is not significant according to the ANOVA analysis [$F(7, 42) = 2.055,\ p > 0.05$]. This is probably caused by the increased variance in the estimates for conditions C1 and C8. The opposite trend compared to the motion-perception gain is an obvious result, as visual lead and lead resulting from the integrating action of the semicircular canals are interchangeable. In Fig. 13d no trend is observed for the visual lag time constant and this is also confirmed by the ANOVA analysis [$F(7, 42) = 0.789,\ p > 0.05$].

The visual-perception time delay significantly increases when the target forcing function power increases [$F(7, 42) = 3.854,\ p < 0.05$]. As can be verified from Fig. 13e this trend is linear [$F(1, 6) = 9.575,\ p < 0.05$]. As the conflict between the visual and physical motion cues increases, it takes more time to process the visual cues. Figure 13f shows that the pitch motion-perception time delay remains constant [$F(7, 42) = 0.631,\ p > 0.05$].

According to Fig. 13g, the neuromuscular damping shows a similar trend as the motion-perception gain when the target power is increased. However, this effect is not significant [$F(7, 42) = 2.292,\ p > 0.05$]. The neuromuscular frequency is significantly affected by the change in forcing function power [$F(7, 42) = 3.545,\ p < 0.05$]. There is a significant linear increasing trend [$F(1, 6) = 7.839,\ p < 0.05$], as can be seen in Fig. 13h.

2. *Variance Accounted For*

Figure 14 illustrates the means and 95% confidence intervals of the VAF for all conditions. The data are adjusted using the subject means to compensate for the between-subject variability. Note that the VAF is between 85 and 90% for all conditions. This implies that 85 to 90% of the variance of the measured control signals can be explained by the linear pilot model, the remaining 10 to 15% is pilot remnant. This percentage of pilot remnant in the control signal is lower compared to the value found in Sec. V.A. This is caused by averaging the time-domain data for the MLE method, reducing the remnant component in the signals. The VAFs for the pure target and disturbance tasks are equal to the VAFs found for the remaining conditions, indicating that fixing some of the parameters did not affect the accuracy of the model fit in the time domain.

3. *Disturbance and Target Open-Loop Response Functions*

Figure 15 gives the disturbance and target open-loop response functions, including the crossover frequencies and phase margins for condition C5 of subject 2. The open-loop estimates are constructed using the estimated pilot frequency response functions and Eqs. (9) and (10). However, the open-loop frequency response functions can also be calculated analytically using the Fourier coefficients of u, δ_e, θ, and e at the input frequencies of the forcing functions. The analytically calculated disturbance and target open-loop responses are also given in Fig. 15 and indicate that the MLE estimates have a high accuracy in the frequency domain.

The means and 95% confidence intervals of the disturbance and target crossover frequencies and phase margins are given in Fig. 16. The between-subject variability is removed by adjusting the data with the subject means. The figure shows that increasing the target forcing function power decreases the disturbance crossover frequency and consequently increases the disturbance phase margin. The ANOVA analysis indicates that the decrease in crossover frequency is significant [$F(6, 36) = 27.699,\ p < 0.05$] with a linear trend [$F(1, 6) = 39.476,\ p < 0.05$], but the increase in phase margin is not [$F(6, 36) = 4.429,\ p > 0.05$]. The target crossover frequency and phase margin remain constant when the power of the forcing functions is varied [$F(6, 36) = 2.054,\ p > 0.05$ and $F(6, 36) = 1.149,\ p > 0.05$].

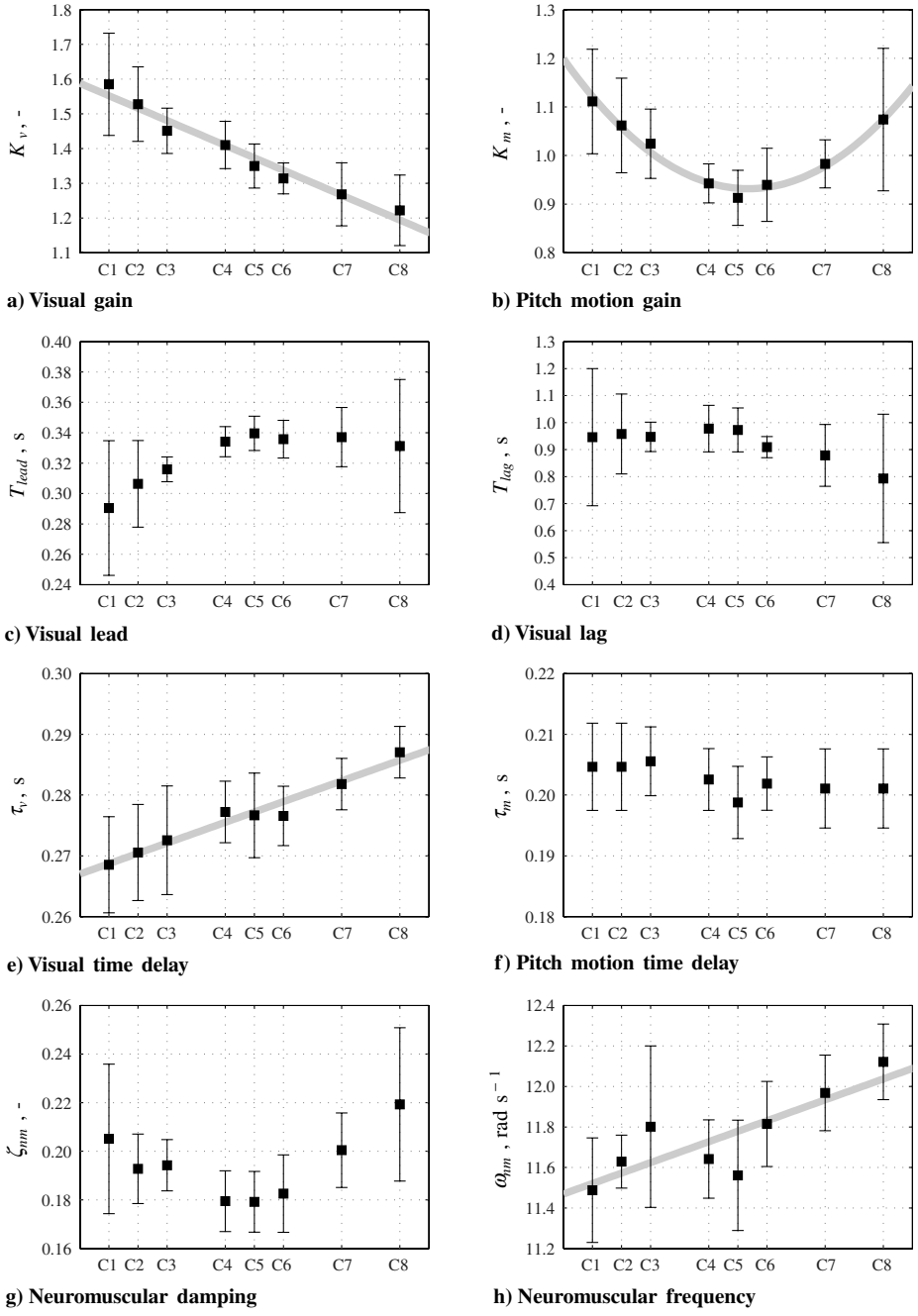

Fig. 13 Means and 95% confidence intervals of the multimodal pilot-model parameters. The data are corrected for between-subject variability. Gray lines indicate significant trends.

Figure 16 shows that for the pure disturbance-rejection task, for which the physical motion cues are fully correlated with the visual cues, the disturbance crossover frequency is found to be the highest. When the power of the target forcing function increases, the correlation between the cues becomes smaller and the disturbance crossover frequency is reduced. The disturbance phase margin is found to increase, indicating increased stability margins for the disturbance-rejection loop. The target crossover frequency and phase margin are not affected by the forcing function power settings. These results were also found in a previous experiment [17].

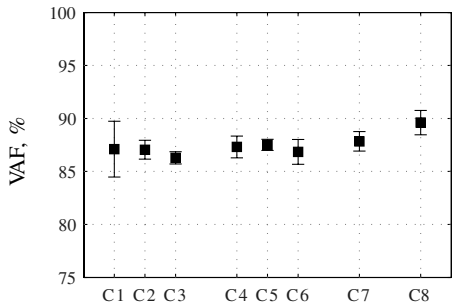

Fig. 14 Means and 95% confidence intervals of the variance accounted for, corrected for between-subject variability.

VI. Discussion

Seven subjects participated in an experiment that investigated the effects of forcing function power settings on pilot performance and control behavior in a combined target-following disturbance-rejection pitch control task. The experiment was performed in the SIMONA Research Simulator at Delft University of Technology. In eight experimental conditions, the pitch control task was varied from a pure disturbance task to a pure target task, with combined tasks in between.

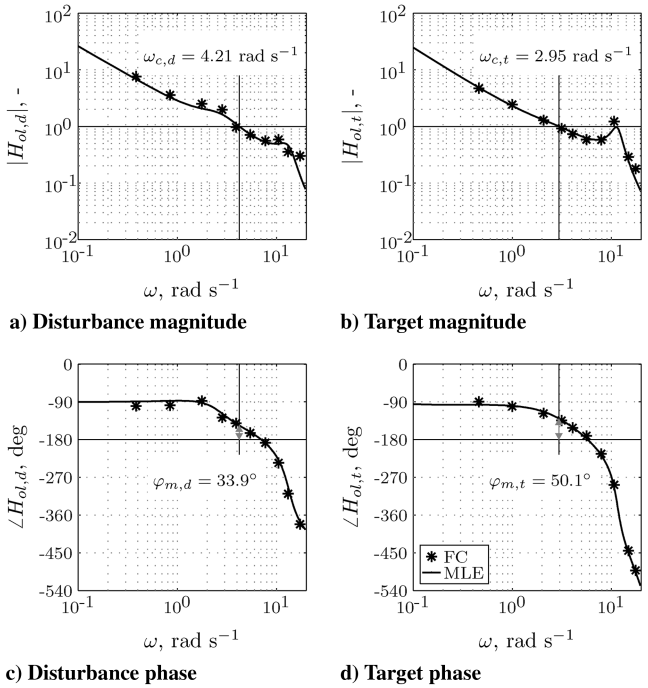

a) Disturbance magnitude **b) Target magnitude**

c) Disturbance phase **d) Target phase**

Fig. 15 Open-loop frequency response functions (subject 2, C5).

Overall, pilot performance degraded significantly for tasks with higher power of the target forcing function. This is a result of the higher performance in decreasing the disturbance variance component in the error signal compared to the target variance component, and can be explained by the fact that the disturbance signal directly influences the physical motion cues. Physical motion cues provide faster lead information on the effect of the disturbance signal, as compared to visual lead, increasing performance. In addition to the decrease in overall performance, pilot control activity is also found to decrease.

The results of the MLE parameter estimation procedure indicate that multimodal pilot control behavior is significantly affected by the power settings of the target and disturbance signals. When the power of the target forcing function becomes higher, the relation between the visual and physical motion cues becomes less evident and an increasing cue conflict arises. The resulting effect is a decrease in visual-perception gain and an increase in visual-perception time delay. The motion-perception gain first decreases, but when the target power becomes dominant, increases again. The opposite effect is seen for the visual lead time constant, as the visual lead and the lead resulting from the integrating action of the semicircular canals are interchangeable. With an increase in target forcing function power, the performance in the attenuation of the disturbance error decreases, as is seen by a decrease in disturbance crossover frequency.

The optimal control analysis proved to be helpful in understanding the theoretically optimal use of the different motion cues for a change in relative power of the forcing functions, giving the limitations of the pilot. The decrease in tracking performance and visual-perception gain were predicted correctly. Also, the initial response of the visual lead time constant and the physical motion-perception gain proved to be correct. The parabolic trend in the motion-perception gain and the visual lead was not predicted correctly, which was most likely caused by the fact that some of the parameters that were fixed in the optimal control analysis (for example, the visual-perception time delay) were seen to change significantly in the experiment. The initial response that was predicted correctly is near the condition that was used to fix some of the parameters in this analysis. In addition, the cost function weighting factors were also fixed and optimized for one condition. It can be expected that as the relation between the motion cues changes, also the internal weighting of the different cues and the control signal changes. These two factors show that due to the many assumptions required to obtain a solvable optimization problem, the use of the results of such a theoretical analysis is limited.

Although marked changes in pilot control strategy are found in the experimental results, the variations in the multimodal pilot-model parameters are only very small. For some parameters the change in magnitude for different experimental conditions is just on the order of 1%. This warrants the use of parameter estimation techniques that can guarantee very accurate parameter estimates, such as the MLE procedure adopted here. In an earlier experiment investigating the influence of forcing function power settings on pilot control behavior, no significant change in control behavior was found [17]. This could have been because of the less accurate parameter estimation techniques used in this research.

No accurate parameter estimates could be achieved for the pure target and disturbance tasks without reducing the number of free parameters in the optimization problem. This is caused by the general requirement of the parameter estimation techniques that both inputs to the pilot model should be sufficiently exciting. When calculating the pilot responses from Fourier coefficients it is even required that the number of forcing functions that need to be inserted into the control loop equal the number of pilot-model inputs. As neighboring conditions for which an accurate fit was possible were available for this experiment, the data from these conditions were used to fix the visual and pitch motion-perception time delays and the neuromuscular frequency. This allowed for an accurate estimate of the remaining parameters for the pure target and disturbance task with an equally high variance accounted for as for the conditions with two forcing functions.

Experimental measurements of the effects of physical motion cues on pilot control behavior during target following and disturbance rejection are not straightforward, as for pure target-following and disturbance-rejection tasks, multimodal pilot control behavior cannot be accurately estimated. In many previous experiments, this was solved by adding a disturbance or target signal with relatively low power in addition to the original target or disturbance signal, respectively. The results of the experiment described in this paper indicate that this strategy can indeed be used, as such an additional signal was found to have only a relatively small effect on pilot performance and control behavior. The experiment also revealed that the additional signal can have very little power, thereby minimizing

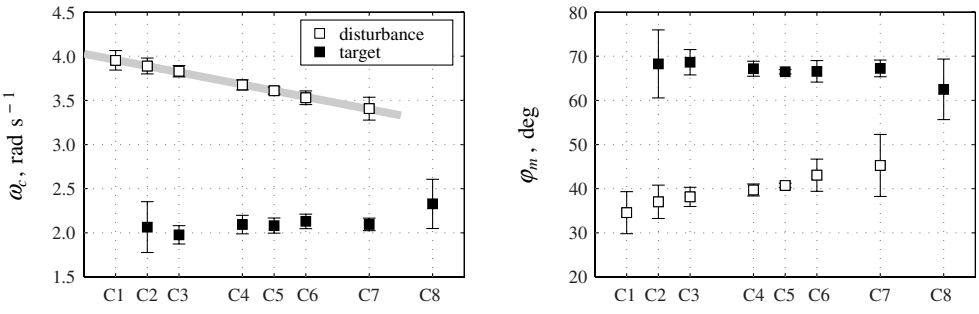

a) Crossover frequency **b) Phase margin**

Fig. 16 Means and 95% confidence intervals of the crossover frequencies and phase margins, corrected for between-subject variability. Gray lines indicate significant trends.

the interference with the dominant task, while still allowing for accurate estimation of pilot-model parameters. Using a target signal with 10% of the total power in addition to a disturbance with 90% of the total power results in multimodal pilot control behavior that is highly similar to control behavior in a pure disturbance task.

VII. Conclusions

In a combined target-following disturbance-rejection aircraft pitch control task, multimodal pilot control behavior is significantly affected by the relative power settings of the target and disturbance forcing functions. With an increase in relative target power, the cue conflict between the visual and physical motion cues increases. This causes a reduction in the visual-perception gain, while the visual-perception time delay becomes higher. The motion-perception gain decreases, but is found to increase again if the target power becomes dominant. As the lead information is the result of the integrating action of the semicircular canals, the change in physical motion gain is counteracted by an opposite trend in the visual lead time constant. The result of this change in control strategy when increasing the target forcing function power is a reduction in tracking performance and control activity. The reduced performance is also apparent from the decrease in disturbance crossover frequency, indicating a decreased attenuation of the disturbance errors in the frequency domain. Despite these effects, multimodal pilot control behavior in a pure target-following or disturbance-rejection task can be evaluated by using a combined target-following disturbance-rejection task with an additional signal with relatively small magnitude. In this case, control behavior is highly comparable to the single forcing function tasks, while still allowing for accurate estimation of the multimodal pilot-model parameters.

Acknowledgments

This research was supported by the Technology Foundation STW, the Applied Science Division of The Netherlands Organisation for Scientific Research (NWO), and the technology program of the Ministry of Economic Affairs.

References

[1] Zaal, P. M. T., Pool, D. M., De Bruin, J., Mulder, M., and Van Paassen, M. M., "Use of Pitch and Heave Motion Cues in a Pitch Control Task," *Journal of Guidance, Control, and Dynamics*, Vol. 32, No. 2, March–April 2009, pp. 366–377. doi:10.2514/1.39953

[2] Van den Berg, P., Zaal, P. M. T., Mulder, M., and Van Paassen, M. M., "Conducting Multi-Modal Pilot Model Identification-Results of a Simulator Experiment," AIAA Paper 2007-6892, 20–23 Aug. 2007.

[3] McRuer, D. T. and Jex, H. R., "A Review of Quasi-Linear Pilot Models," *IEEE Transactions on Human Factors in Electronics*, Vol. HFE-8, No. 3, 1967, pp. 231–249. doi:10.1109/THFE.1967.234304

[4] Stapleford, R. L., Peters, R. A., and Alex, F. R., "Experiments and a Model for Pilot Dynamics with Visual and Motion Inputs," NASA Contractor Rept. CR-1325, 1969.

[5] Van Paassen, M. M. and Mulder, M., "Identification of Human Operator Control Behaviour in Multiple-Loop Tracking Tasks," *Proceedings of the Seventh IFAC/IFIP/IFORS/IEA Symposium on Analysis, Design and Evaluation of Man-Machine Systems, Kyoto Japan*, Pergamon, Kidlington, 16–18 Sept. 1998, pp. 515–520.

[6] Nieuwenhuizen, F. M., Zaal, P. M. T., Mulder, M., Van Paassen, M. M., and Mulder, J. A., "Modeling Human Multichannel Perception and Control Using Linear Time-Invariant Models," *Journal of Guidance, Control, and Dynamics*, Vol. 31, No. 4, July–Aug. 2008, pp. 999–1013. doi:10.2514/1.32307

[7] Zaal, P. M. T., Pool, D. M., Chu, Q. P., Van Paassen, M. M., Mulder, M., and Mulder, J. A., "Modeling Human Multimodal Perception and Control Using Genetic Maximum Likelihood Estimation," *Journal of Guidance, Control, and Dynamics*, Vol. 32, No. 4, 2009, pp. 1089–1099. doi:10.2514/1.42843.

[8] Jex, H. R., Magdaleno, R. E., and Junker, A. M., "Roll Tracking Effects of *G*-Vector Tilt and Various Types of Motion Washout," *Fourteenth Annual Conference on Manual Control*, University of Southern California, Los Angeles, CA, 25–27 April 1978, pp. 463–502.

[9] Van der Vaart, J. C., "Modelling of Perception and Action in Compensatory Manual Control Tasks," Ph.D. Dissertation, Faculty of Aerospace Engineering, Delft University of Technology, 1992.

[10] Hosman, R. J. A. W., "Pilot's Perception and Control of Aircraft Motions," Ph.D. Dissertation, Faculty of Aerospace Engineering, Delft University of Technology, 1996.

[11] Pool, D. M., Mulder, M., Van Paassen, M. M., and Van der Vaart, J. C., "Effects of Peripheral Visual and Physical Motion Cues in Roll-Axis Tracking Tasks," *Journal of Guidance, Control, and Dynamics*, Vol. 31, No. 6, Nov.–Dec. 2008, pp. 1608–1622. doi:10.2514/1.36334

[12] Kaljouw, W. J., Mulder, M., and Van Paassen, M. M., "Multi-Loop Identification of Pilot's Use of Central and Peripheral Visual Cues," AIAA Paper 2004-5443, 16–19 Aug. 2004.

[13] Steurs, M., Mulder, M., and Van Paassen, M. M., "A Cybernetic Approach to Assess Flight Simulator Fidelity," AIAA Paper 2004-5442, 16–19 Aug. 2004.

[14] Berntsen, M. F. F., Mulder, M., and Van Paassen, M. M., "Modelling Human Visual Perception and Control of the Direction of Self-Motion," AIAA Paper 2005-5893, 15–18 Aug. 2005.

[15] Löhner, C., Mulder, M., and Van Paassen, M. M., "Multi-Loop Identification of Pilot Central Visual and Vestibular Motion Perception Processes," AIAA Paper 2005-6503, 15–18 Aug. 2005.

[16] Zaal, P. M. T., Nieuwenhuizen, F. M., Mulder, M., and Van Paassen, M. M., "Perception of Visual and Motion Cues During Control of Self-Motion in Optic Flow Environments," AIAA Paper 2006-6627, 21–24 Aug. 2006.

[17] Duppen, M., Zaal, P. M. T., Mulder, M., and Van Paassen, M. M., "Effects of Motion on Pilot Behavior in Target, Disturbance and Combined Tracking Tasks," AIAA Paper 2007-6894, 20–23 Aug. 2007.

[18] Groot, T., Damveld, H. J., Mulder, M., and Van Paassen, M. M., "Effects of Aeroelasticity on the Pilots Psychomotor Behavior," AIAA Paper 2006-6494, 21–24 Aug. 2006.

[19] De Bruin, J., Mulder, M., Van Paassen, M. M., Zaal, P. M. T., and Grant, P. R., "Pilot's Use of Heave Cues in a Pitch Control Task," AIAA Paper 2007-6895, 20–23 Aug. 2007.

[20] Zaal, P. M. T., Pool, D. M., Mulder, M., and Van Paassen, M. M., "New Types of Target Inputs for Multi-Modal Pilot Model Identification," AIAA Paper 2008-7106, 2008.

[21] Berkouwer, W. R., Stroosma, O., Van Paassen, M. M., Mulder, M., and Mulder, J. A., "Measuring the Performance of the SIMONA Research Simulator's Motion System," AIAA Paper 2005-6504, 15–18 Aug. 2005.